

# Photoabsorption and photofragmentation studies of $\text{Ar}_n^+$ cluster ions

Nancy E. Levinger, Douglas Ray, Michael L. Alexander,<sup>a)</sup> and W. C. Lineberger  
*Department of Chemistry and Biochemistry and Joint Institute for Laboratory Astrophysics, University of Colorado and National Bureau of Standards, Boulder, Colorado 80309*

(Received 24 June 1988; accepted 29 July 1988)

We have measured the photoabsorption spectra of mass selected  $\text{Ar}_n^+$  clusters,  $n = 3-40$ , from 355–1064 nm. The smaller clusters,  $n < 15$ , display a visible photoabsorption spectrum similar to  $\text{Ar}_3^+$ , i.e., a broad, intense band peaking near 520 nm. From  $n = 15-20$  this photoabsorption band shifts smoothly to a longer wavelength, peaking near 600 nm for  $\text{Ar}_{20}^+$ . This band does not change appreciably as  $n$  increases from 20 to 40. These results clearly demonstrate that the  $\text{Ar}_n^+$  clusters have photophysical properties quite different from those of  $\text{Ar}_2^+$ . We have also studied the photoabsorption and subsequent photofragmentation of  $\text{Ar}_n^+$  cluster ions,  $n = 3-60$ , at selected visible wavelengths. The ionic photofragment distributions both indicate that photofragmentation proceeds through the loss of individual Ar atoms and place an upper bound of 90 meV on the cluster ion binding energy in the large cluster limit.

## I. INTRODUCTION

Investigations of rare gas clusters have been prevalent since cluster investigations began several decades ago.<sup>1-3</sup> The closed shell nature of the rare gas atom constituents create an inviting cluster for both theory and experiment. Unfortunately, the ionization of neutral clusters, which is required to mass analyze them, generally results in fragmentation,<sup>4-7</sup> thereby placing only a lower limit on the mass of the neutral cluster. Indeed it has been amply demonstrated that the abundance anomalies, or magic numbers, in neutral cluster mass spectra are principally due to the ions formed prior to mass analysis and not the distribution of neutral clusters.<sup>5-16</sup> Thus, although neutral rare gas clusters are well suited to theoretical studies, they are somewhat problematic for detailed experiments on the transition from gas phase to condensed phase behavior. This has led to both experimental<sup>5-12</sup> and theoretical<sup>13-20</sup> interest in the rare gas cluster ions themselves.

One of the unresolved questions regarding the  $\text{Ar}_n^+$  cluster ions is that of the basic electronic structure of the clusters, viz., what is the extent of charge delocalization? Most calculations have assumed that  $\text{Ar}_2^+$  is the ionic core of the clusters,<sup>13-15,17</sup> although one study has suggested that  $\text{Ar}^+$  is the ionic core.<sup>10</sup> Recently DIM (diatomics-in-molecules) calculations have been presented<sup>16,19</sup> which indicate that  $\text{Ar}_3^+$  is the core of the cluster ions smaller than  $\text{Ar}_{14}^+$ . Experimental evidence regarding this question is indirect; typically mass spectra have been interpreted using hard sphere packing models under the assumption that  $\text{Ar}_2^+$  is the core. In this work we employ a direct method to examine the electronic structure of the  $\text{Ar}_n^+$  cluster ions, namely measurement of the photoabsorption spectra. As the photoabsorption spectra of  $\text{Ar}^+$ ,<sup>21</sup>  $\text{Ar}_2^+$ ,<sup>22-25</sup> and  $\text{Ar}_3^+$ <sup>26</sup> are all known, measurement of the photoabsorption spectra of the large cluster ions can provide an answer to this question.

Photofragmentation studies of cluster ions can offer in-

sights into the energetics of the cluster ions and the unimolecular decay dynamics of the energized cluster. Several photofragmentation studies of cluster ions have appeared recently.<sup>27-36</sup> In all the cases studied photofragmentation proceeds via the loss of monomers or small neutral clusters. Some of these data have been interpreted as evidence that the abundance anomalies in ionic cluster mass spectra are due to the energetics of the cluster ions.<sup>30</sup> In addition, in some cases the  $\text{X}_k^+ - \text{X}$  dissociation energy for the large cluster ions has been estimated.<sup>28,37</sup>

In this work we present an extensive set of measurements on the photophysical properties of the  $\text{Ar}_n^+$  cluster ions. The data are obtained by mass selecting the cluster ion of interest prior to interaction with laser radiation, and mass analyzing and detecting the resulting ionic photofragments. Laser wavelength and initial cluster size are independently variable offering unique information regarding the transition between gas phase and condensed phase behavior.

## II. EXPERIMENTAL METHOD

Figure 1 displays a schematic of the apparatus employed in these experiments. A detailed description appears elsewhere<sup>38,39</sup>, therefore, only a brief description is given here. The  $\text{Ar}_n^+$  cluster ions were created by crossing a pulsed free jet expansion of argon with a continuous 1 keV beam of electrons. Expansion conditions were chosen such that neutral clustering is not extensive. The primary ions formed following electron beam excitation were  $\text{Ar}^+$ ,  $\text{Ar}_2^+$ , and  $\text{Ar}_3^+$ . The larger clusters grew by sequential ion-molecule association reactions while drifting with the unskimmed expansion.<sup>40</sup> The stagnation pressure of neat Ar gas behind the 0.8 mm diameter orifice was 2 atm. The pulsed valve (General Valve series 9) was cooled to 200 K by four thermoelectric coolers (Melcor series FC). Typically, the valve pulse length was 500  $\mu\text{s}$ . The 1000 eV, 200  $\mu\text{A}$  electron beam intersected the pulsed expansion  $< 0.1$  cm below the valve orifice. Placement of the electron beam in the high density region of the expansion, where growth via nucleation about the initially

<sup>a)</sup> Present address: Los Alamos National Laboratory MS M888, Los Alamos, NM 87545.

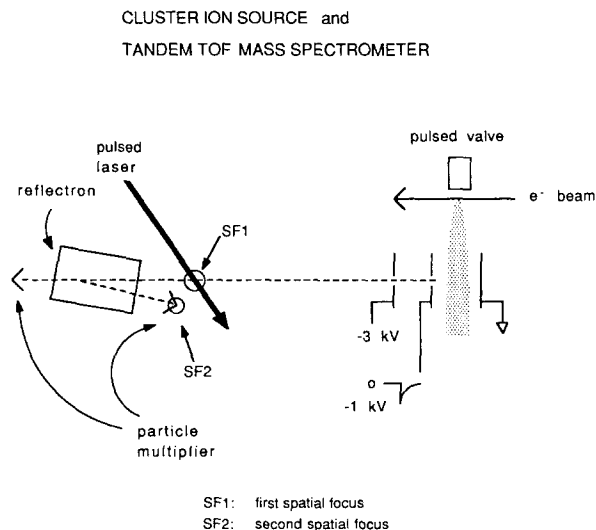


FIG. 1. Schematic diagram of the cluster ion source and tandem TOF mass spectrometer. Ions are separated in time according to their mass at SF1, where they interact with the pulsed laser. The reflectron field is adjusted to refocus either the initial ions or ionic fragments of a selected mass at SF2 where the ions are detected by a particle multiplier.

formed ions can occur and inelastic collisions can effect relaxation of the cluster ions, was crucial for the production of large cluster ions. In this configuration large cluster ions,  $n \leq 60$ , were produced with high intensity.

The ions drift 20 cm from the valve orifice before pulse extraction into a tandem time-of-flight (TOF) mass spectrometer. Mass selected ions are intersected by laser pulses from a Nd:YAG laser or a Nd:YAG pumped dye laser (Quanta Ray DCR-3 and PDL-1) at the spatial focus of the primary TOF mass analyzer (SF1 in Fig. 1). Following the laser interaction, a reflectron<sup>41</sup> type secondary TOF mass analyzer is employed. By adjusting the reflectron field, the initial ions *or* ionic fragments of a selected mass can be refocused at SF2 (see Fig. 1) and detected by the particle multiplier located there. Neutral fragments, which are not affected by the reflectron, traverse it and strike a separate particle multiplier.

Photodissociation cross sections were measured via the photoinduced depletion of the mass selected ions. Depletion measurements are less sensitive and more difficult than cross section measurements based on the appearance of photofragments, but were employed here to eliminate systematic effects due to the mass dependent detection efficiencies of the particle multipliers. Photodissociation cross sections were obtained by refocusing the initial ions onto the particle multiplier at SF2 and measuring the photoinduced depletion of the mass selected ions. The observed depletion was normalized to the laser pulse energy on every valve opening. These data were collected with a multichannel gated integrator (LeCroy 2249SG) for 200 valve openings with the laser striking the selected ions and 200 with the laser blocked. All cross section data were obtained with the laser fluence selected to limit the depletion of the mass selected ion to less than 20%. The laser fluences used varied from 0.05 to 1.5  $\text{mJ}/\text{cm}^2$  depending on the wavelength.

The photofragmentation data were obtained by measur-

ing the production of the mass selected ionic photofragments. The reflectron was adjusted to refocus the selected ionic photofragments at SF2 and the photoinduced fragment ion current was measured there by the particle multiplier. These data were collected with a transient digitizer/signal averager (Transiac 2001S/4100) for 300 valve openings with the laser striking the selected ions and 300 with the laser blocked for each mass selected ionic photofragment. The photofragment mass peaks were integrated and normalized to the total photofragment ion intensity from a given mass initial ion to yield relative branching ratios. Multiphoton effects were easily identified as laser fluence dependent fragmentation patterns, allowing the extent of multiphoton processes to be determined accurately (see Sec. III B). All photofragmentation data were obtained with the laser fluence selected to minimize multiphoton effects. The laser fluences used varied from 1 to 15  $\text{mJ}/\text{cm}^2$  depending on the wavelength.

### III. RESULTS AND DISCUSSION

Figure 2 displays a mass spectrum of  $\text{Ar}_n^+$  clusters generated under the conditions described above. While these conditions can be adjusted to move the envelope of the distribution of cluster ions to smaller or larger cluster sizes, the intensity anomalies (relative to neighboring peaks) observed in the mass spectrum in the region from  $\text{Ar}_{14}^+$  to  $\text{Ar}_{30}^+$  (e.g., high at  $n = 14, 16, 21, 27$ , very low at  $n = 20$ ) are independent of these conditions. These intensity anomalies occur at the same cluster sizes as those reported in the electron impact ionization of neutral  $\text{Ar}_n$  clusters in a collisionless region,<sup>5,6,9,11,42</sup> but differ from those reported in the generation of  $\text{Ar}_n^+$  clusters in a high pressure corona discharge source<sup>10</sup> (e.g., high at 19, 23, 26, and 29). The reason for this difference is not known at present.

Two distributions of cluster ions appear in this mass spectrum. The primary, most intense, distribution is comprised of the  $\text{Ar}_n^+$  cluster ions of interest. The decay of metastable cluster ions produces a second distribution of mass peaks; the ionic decay products appear visually as a weaker

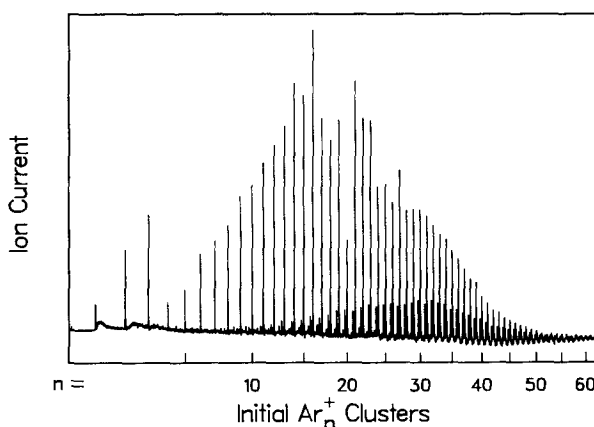


FIG. 2. TOF mass spectrum of the initial  $\text{Ar}_n^+$  cluster ions. The mass spectrum was obtained under conditions described in the text. The signal arises from ions striking the particle multiplier located at SF2.

distribution, peaking near  $\text{Ar}_{30}^+$ . These ions result from the loss of a single Ar atom from the following cluster ion in the primary distribution, the dissociation occurring in the field free region of the first TOF mass analyzer. For example, the largest peak between  $\text{Ar}_{19}^+$  and  $\text{Ar}_{20}^+$  results from the decay of metastable  $\text{Ar}_{20}^+$  into  $\text{Ar}_{19}^+$  and an Ar atom after acceleration but prior to entering the reflectron. The remaining peaks in the mass spectrum are due to various impurities with Ar atoms clustered to them, not to the loss of more than one Ar atom from metastable  $\text{Ar}_n^+$  clusters. Mass peaks attributable to doubly or triply charged argon clusters have not been observed with this apparatus. In Secs. III A and III B, we describe in some detail the photoabsorption and photofragmentation studies on selected  $\text{Ar}_n^+$  ions from such a mass distribution.

### A. Photoabsorption cross section

Photodissociation cross section measurements of several selected  $\text{Ar}_n^+$  cluster ions from  $\text{Ar}_3^+$  to  $\text{Ar}_{40}^+$  were made at various wavelengths from 355 to 1064 nm. The photodissociation cross sections of these  $\text{Ar}_n^+$  cluster ions at 510, 575, and 620 nm are shown as a function of cluster ion size in Fig. 3. There is a substantial variation of the photodissociation cross section with cluster size at all of these wavelengths. The data at 575 and 620 nm show a sharp increase in the photoabsorption cross section occurring between  $\text{Ar}_{15}^+$  and  $\text{Ar}_{20}^+$ . If the change in photodissociation cross section were due to an additive solvation shift of the  $\text{Ar}_3^+$  band from  $\text{Ar}_3^+$  to  $\text{Ar}_{20}^+$ , the range of cluster sizes over which the large change in cross section occurred would be wavelength dependent. This is clearly not in consonance with the data presented in Fig. 3. We conclude from these data that the photodissociation cross section remains relatively invariant from  $\text{Ar}_3^+$  to  $\text{Ar}_{15}^+$ , changes from  $\text{Ar}_{15}^+$  to  $\text{Ar}_{20}^+$ , and remains constant for cluster ions from  $\text{Ar}_{20}^+$  to  $\text{Ar}_{40}^+$ .

A detailed photodissociation cross section was measured for  $\text{Ar}_{23}^+$ , chosen as representative of the photodissociation cross section of the large  $\text{Ar}_n^+$  clusters. It is displayed in Fig. 4 along with our previously reported<sup>26</sup> photoabsorption cross section of  $\text{Ar}_3^+$ , which is representative of the photodissociation cross section of the small  $\text{Ar}_n^+$  cluster ions. The  ${}^2\Sigma_u^+ \leftarrow {}^2\Sigma_g^+$  dissociative transition<sup>23-25</sup> of  $\text{Ar}_2^+$  is also displayed.  $\text{Ar}_2^+$  also has a  ${}^2\Sigma_u^+ \leftarrow {}^2\Pi_g$  dissociative transition which is too weak ( $2 \times 10^{-19} \text{ cm}^2$  at the peak near 720 nm)<sup>22</sup> to be visible in this figure.

These measurements of the photodissociation cross section can be used to infer the absolute photoabsorption cross section of the cluster ions. Two conditions must be met for this inference to be valid. First, the quantum yield for photodissociation (i.e., the photodestruction of the initial ion) must be known at all wavelengths of interest. The energy of a visible photon is certainly much larger than the energy binding an Ar atom to the cluster and the transition is probably to a repulsive surface (in analogy with  $\text{Ar}_3^+$ ).<sup>19,43</sup> We suggest that the absorber is photodissociated within the cluster and that the nascent fragments either escape or are captured by the cluster. Clearly escape is equivalent to dissociation and capture will result in energy redistribution followed by uni-

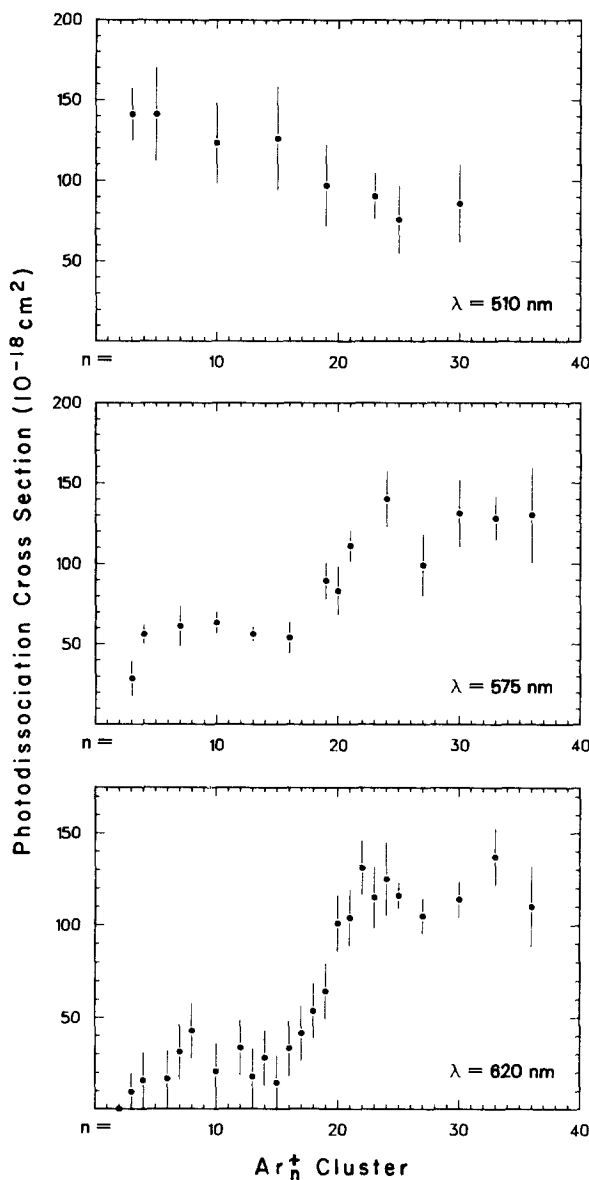


FIG. 3. Absolute photodissociation cross section of  $\text{Ar}_n^+$  as a function of cluster size at 510, 575, and 620 nm. The error bars indicate one standard deviation statistical uncertainty. The uncertainty in the absolute cross section is a factor of 2. All of these data were taken using the depletion method described in the text.

molecular dissociation. Thus, we contend that the quantum yield for photodissociation is unity throughout the visible region.

The second requirement is that dissociation must occur prior to mass analysis in the secondary TOF mass spectrometer. Given the large excess energy in the cluster following photoabsorption, dissociation (i.e., the loss of at least one Ar atom) is very likely to occur within the approximately  $1 \mu\text{s}$  between the spatial focus of the first TOF mass analyzer and the entrance of the reflectron. If dissociation occurred while the initial ions were in the reflectron, i.e., on a microsecond time scale, some of the ionic fragments would arrive at SF2 later in time due to their increased residence time in the reflectron. This would lead to a time asymmetry in the ionic photofragment signals. Since we have not observed any

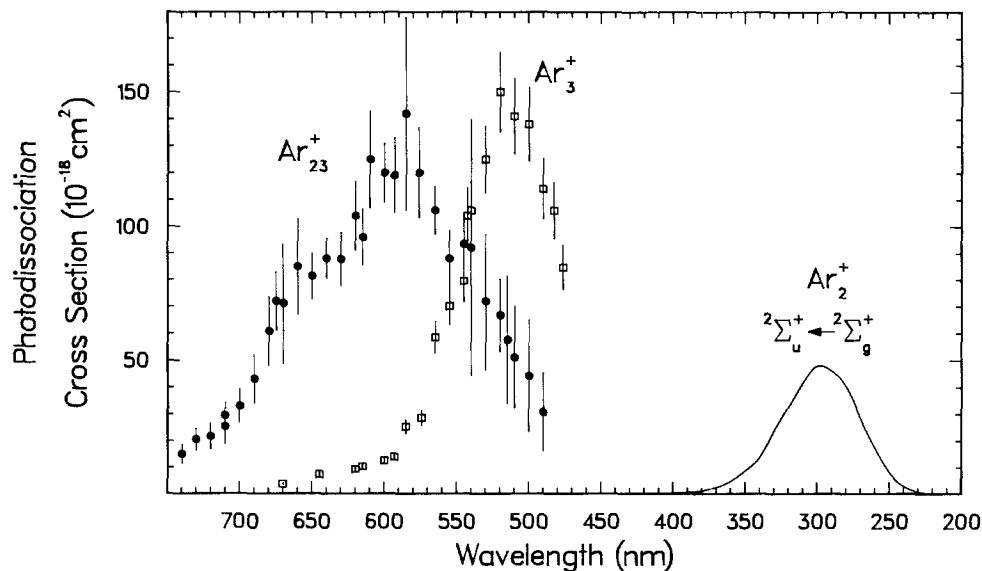


FIG. 4. Absolute photodissociation cross sections of  $\text{Ar}_2^+$ ,  $\text{Ar}_3^+$ , and  $\text{Ar}_{23}^+$ . The error bars indicate one standard deviation statistical uncertainty. The uncertainty in the absolute cross sections of  $\text{Ar}_3^+$  and  $\text{Ar}_{23}^+$  is a factor of 2. The  $\text{Ar}_2^+$  cross section is from Ref. 25.

asymmetric line shapes in the photofragment mass spectra we infer that dissociation is complete on a submicrosecond time scale. Indeed, an RRK model calculation predicts that the loss of one Ar atom will occur on a picosecond time scale for  $\approx 2$  eV of excess energy. Having satisfied both criteria we conclude that the measured photodissociation cross sections are equivalent to the absolute photoabsorption cross section.

From the photodissociation data (Figs. 3 and 4) and the discussion above we conclude that the absolute photoabsorption cross section of  $\text{Ar}_n^+$  remains relatively constant from  $\text{Ar}_3^+$  to  $\text{Ar}_{15}^+$ ; the peak shifts smoothly  $2300\text{ cm}^{-1}$  to lower energy from  $\text{Ar}_{15}^+$  to  $\text{Ar}_{20}^+$ , and is constant for cluster ions between  $\text{Ar}_{20}^+$  and  $\text{Ar}_{40}^+$ . Furthermore, the photoabsorption spectra for  $n = 20\text{--}40$  are broader than the photoabsorption spectra for  $n = 3\text{--}15$  ( $4500\text{ cm}^{-1}$  FWHM vs  $2600\text{ cm}^{-1}$  FWHM).

Consideration of the diatomics-in-molecules calculations on  $\text{Ar}_n^+$  clusters by Kuntz and Valldorf<sup>19</sup> provides some insight into the change in electronic structure which occurs as a function of cluster size. The major finding of the calculations is that the ground states of the  $\text{Ar}_n^+$  cluster ions consist of a small ionic molecule, trimer, or tetramer ion, surrounded by nearly neutral atoms. Thus,  $\text{Ar}_2^+$  is *not* the core of the cluster ion and the charge does not spread over the entire cluster ion as the cluster size increases. From  $\text{Ar}_4^+$  to  $\text{Ar}_{13}^+$  the charge is calculated<sup>19</sup> to be localized on a linear symmetric trimer ion core. At  $\text{Ar}_{14}^+$  the positive charge begins to delocalize onto a fourth atom, creating a linear asymmetric tetramer ion surrounded by neutral Ar atoms. The calculations indicate that further delocalization onto the fourth atom continues until  $\text{Ar}_{19}^+$ . This range of cluster ions is approximately the same range over which we observe the shift in photoabsorption cross section. The calculations also predict that the large clusters have many more electronic states than the smaller clusters, which may explain the broader photoabsorption band we observe for the larger clusters. The DIM calculations further indicate that the excited electronic states of the clusters do not, in general, correspond to an electronically excited trimer ion interacting

with the surrounding Ar atoms but to clusters with a somewhat delocalized positive charge. Based on the similarity of the photoabsorption cross sections of  $\text{Ar}_3^+$  through  $\text{Ar}_{15}^+$  it appears that at least some excited electronic states exist in these clusters which resemble an excited trimer ion surrounded by neutral Ar atoms. Our data do not allow us to comment on the extent of delocalization in the excited electronic states of the larger clusters. Overall, our measurements are consistent with the predictions of the DIM calculations, and indicate that caution is warranted in the use of the model of  $\text{Ar}_n^+$  clusters based on  $\text{Ar}_2^+$  surrounded by neutral Ar atoms.

It is also interesting to consider the properties of holes in rare gas crystals in relation to the properties of the  $\text{Ar}_n^+$  clusters. LeComber *et al.*<sup>44</sup> interpret the extremely low hole mobilities measured in rare gas crystals as an indication of the existence of self-trapped holes. In general, a hole in a pure crystal will be self-trapped, or localized, when the gain in energy due to localization is larger than the strain energy induced by the displacement of the nearby atoms from their equilibrium lattice sites. Calculations confirm that holes are localized in rare gas crystals and further predict that they can be localized on either dimer<sup>45–48</sup> or trimer<sup>48</sup> centers. Umehara<sup>48</sup> predicts that the holes localized on trimer centers are slightly more stable than those localized on dimer centers, and furthermore that holes localized over larger centers are unstable relative to free holes. This result is attributed to an increased strain energy rather than a decreased localization energy for these large centers. Large clusters, however, may be able to support charge localization on centers larger than three atoms since the strain energy is reduced relative to that in the Ar crystal. As discussed above, our data do not allow us to comment on the extent of delocalization in the excited electronic states of the larger clusters.

## B. Photofragmentation studies on $\text{Ar}_n^+$

Photofragmentation studies were conducted on  $\text{Ar}_3^+$  through  $\text{Ar}_{60}^+$  at three different photon energies, 2.33 (532

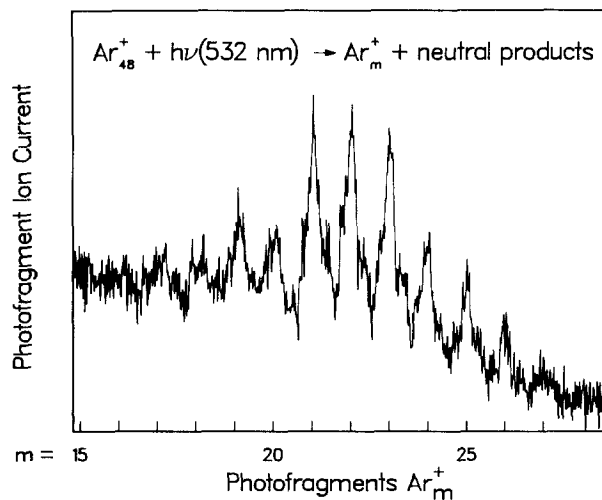


FIG. 5. The ionic photofragments from the photodissociation of  $\text{Ar}_{48}^+$  at 2.33 eV (532 nm). Absorption of a second photon results in the appearance of ionic fragments much smaller than, and easily distinguishable from, the fragments shown here.

nm), 1.77 (700 nm), and 1.55 eV (820 nm). The ionic photofragment distribution resulting from absorption of one 2.33 eV photon by  $\text{Ar}_{48}^+$  is shown in Fig. 5. At increased laser fluence, absorption of a second 2.33 eV photon results in the

appearance of a distribution of ionic fragments centered near  $\text{Ar}_6^+$ , much smaller than, and easily distinguishable from, the fragments observed from one photon absorption. A representation of the ionic photofragment distribution from each initial cluster ion following absorption of one 2.33 eV photon is displayed in Fig. 6. Also represented in Fig. 6 is the ionic photofragment distribution from each initial cluster ion following absorption of one 1.55 eV photon. The fragment ions are recorded on the horizontal axis and the initial cluster size is displayed on the depth axis of the figure. Data corresponding to excitation at 1.77 eV are similar to the data in Fig. 6, with the ionic photofragment distributions occurring between those resulting from 2.33 and 1.55 eV excitation.<sup>49</sup>

There are three prominent features of the data presented in Fig. 6. First, the average size of the photofragment ions resulting from photodissociation increases with the size of the initial cluster ion. Second, of the photofragment ions which could be formed from the photodissociation of an absorbing cluster ion (limited by energy and particle number conservation), only a narrow distribution is observed. Finally, the  $\text{Ar}_{20}^+$  photofragment is much less intense than the other ionic photofragments. This behavior results in a prominent "valley" in the photofragment distributions, the position of which is clearly *independent* of photon energy.

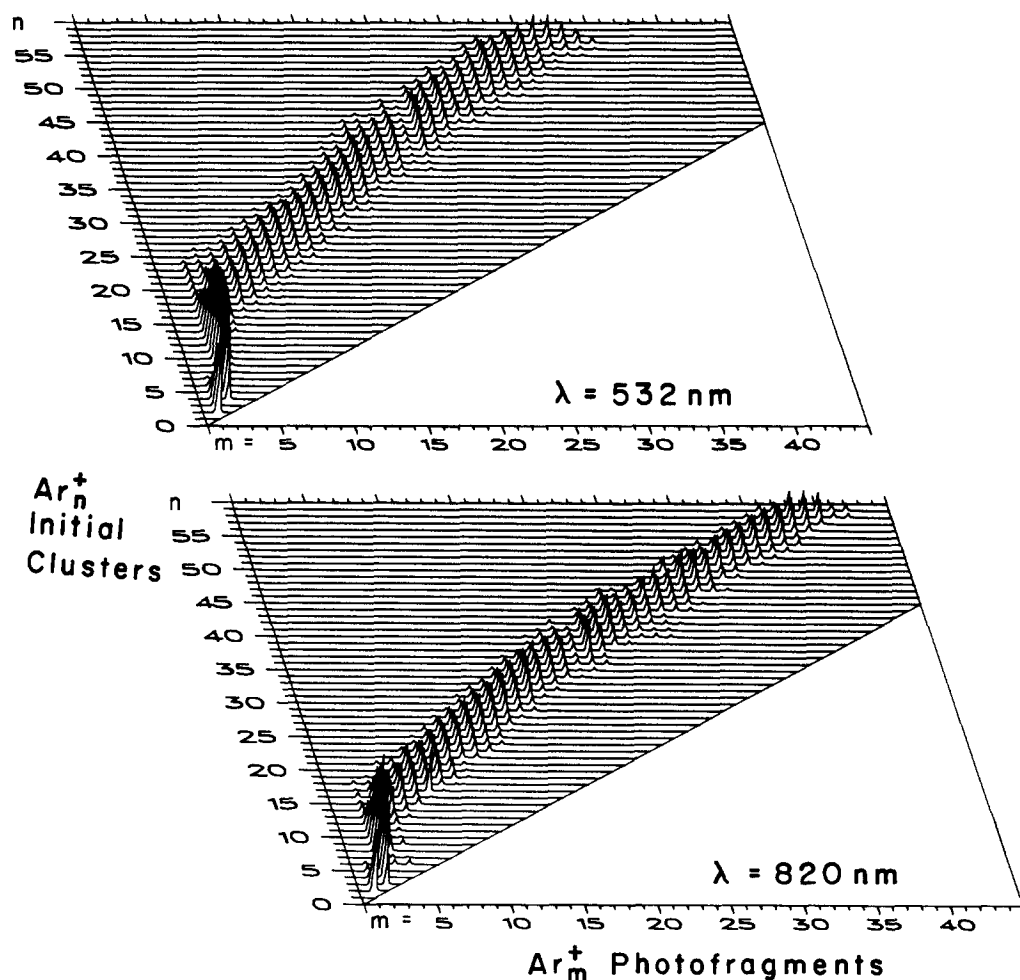


FIG. 6. The ionic photofragments from the photodissociation of  $\text{Ar}_n^+$  as a function of initial cluster size at 2.33 eV (532 nm) and 1.55 eV (820 nm). The average size of the fragments increases with initial cluster size and decreases with excitation energy. Note also that only a narrow distribution of fragments is observed.

Each of these features must be explained by any model of the photofragmentation process.

There are two limiting processes by which photofragmentation can occur. In an evaporative mechanism<sup>50</sup> the ejection of the neutral atoms is determined principally by the total energy content of the cluster. This mechanism resembles the RRKM model for unimolecular dissociation and is based on the concept of energy randomization in the cluster unrestricted by dynamical effects. The other possible limit is impulsive, or direct, fragmentation and involves the simultaneous dissociation of the energized cluster ion into multiple fragments. In the direct process, dynamical effects dominate the fragmentation with the total energy content playing a secondary role. The actual mechanism is likely a combination of these two limiting cases. For example, it is possible that, following excitation, the initial atoms are ejected simultaneously by an impulsive mechanism, while the final atoms are lost sequentially via evaporation.

Both limiting cases have been reported in the photofragmentation behavior of large ionic clusters. The principal difference in the cases is the ratio of the excitation energy to the strength of the interaction between the monomers. Thus weakly interacting monomers, e.g.,  $\text{CO}_2$  molecules, appear to be ejected individually in an evaporative mechanism following visible and near UV excitation,<sup>28,30</sup> while strongly interacting monomers, e.g., C atoms, appear to be ejected impulsively in various forms, e.g., as C atoms,  $\text{C}_2$  or  $\text{C}_3$ ,<sup>34,35</sup> following visible and near UV excitation. Argon atoms are only weakly interacting and are therefore expected to be ejected individually via an evaporative mechanism following visible excitation. Careful consideration of the data is required, however, since recent work on  $\text{Br}_2$  and  $\text{Br}_2^-$  photodissociated within clusters<sup>38,51,52</sup> suggests that the detailed dynamics may be important in the photofragmentation process.

In order to elucidate the photofragmentation mechanism, it is useful to characterize the ionic photofragment distributions by the average number of neutral atoms ejected following photoabsorption. This quantity is plotted in Fig. 7 as a function of absorbing cluster ion size for the three different excitation energies employed. For the large cluster ions the average number of neutral atoms ejected is independent of cluster size and linearly dependent on the photon energy. This behavior indicates that the photofragmentation of large clusters is controlled principally by the *amount* of energy deposited in the cluster and therefore suggests that an evaporative mechanism governs photofragmentation in the large clusters. For the smaller cluster ions the average number of neutral atoms lost is roughly proportional to the size of the initial cluster ion and is independent of the photon energy. This behavior does not eliminate an evaporative mechanism from consideration, however, since for the small clusters the effects of particle number conservation dominate the ionic fragment distributions. Thus, following excitation, the small clusters eject Ar atoms until  $\text{Ar}_3^+$  or  $\text{Ar}_2^+$  is reached. Given their relatively large dissociation energies (0.22<sup>53</sup> and 1.28 eV,<sup>64</sup> respectively) these fragments can store energy effectively. The data support this explanation: the major ionic photofragments from clusters smaller than  $\text{Ar}_{15}^+$  are  $\text{Ar}_2^+$  or  $\text{Ar}_3^+$ , independent of photon energy. Obviously if the ionic fragments remain nearly the same while the initial cluster size increases, the average number of neutral atoms lost will be roughly proportional to the size of the initial cluster ion.

Although we do not mass analyze the neutral photofragmentation products, examination of the ionic photofragmentation products allows us to demonstrate that the dominant photofragmentation pathway involves the loss of individual Ar atoms. If the loss of small neutral Ar clusters were a major decay channel the ionic fragment distributions would be modulated rather than smooth. For example, if

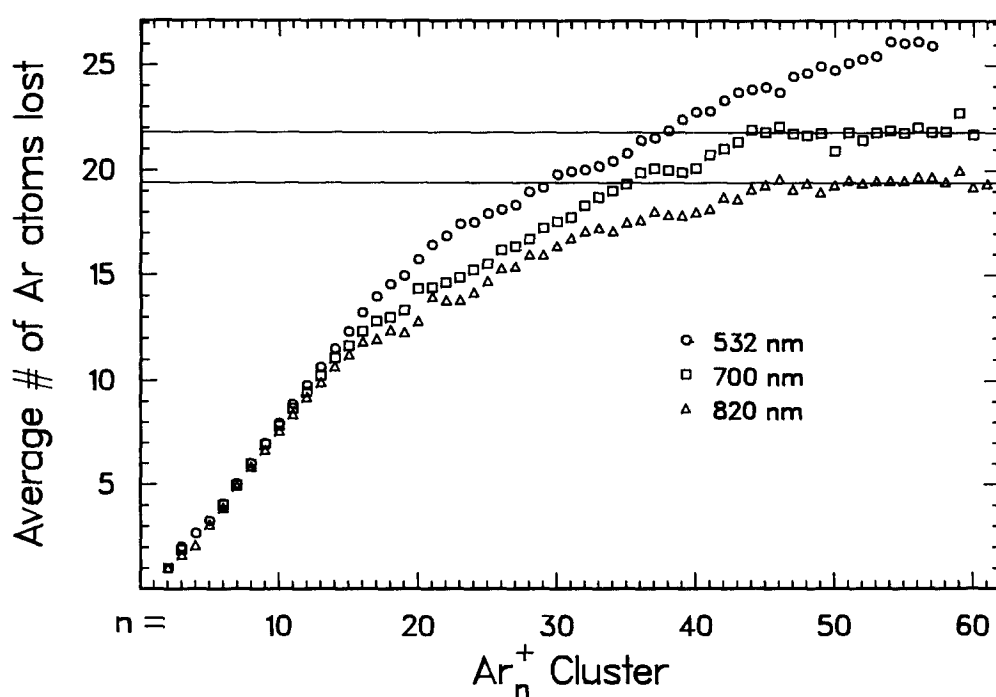


FIG. 7. The average number of neutral Ar atoms lost by  $\text{Ar}_n^+$  following absorption of a 2.33, 1.77, or 1.55 eV photon as a function of initial cluster size. The horizontal lines indicate the asymptotic value at two excitation energies.

photoexcited  $\text{Ar}_{48}^+$  decayed primarily through the loss of argon dimers, the fragment ions with an even number of atoms would be much more abundant than those with an odd number of atoms. The modulation would also be expected to be independent of excitation energy. It is apparent from Fig. 5 and the other ionic photofragmentation data that there is no modulation of the ionic fragment distributions. There is some irregularity in the distributions, but it is excitation energy dependent and due to the energetics of the ionic photofragments. This will be discussed in detail later in this section.

While we cannot rule out the loss of neutral clusters as a minor channel in the decay process, we can place an upper limit of 5% on the loss of neutral clusters. As discussed above, the only channel we observe in the decay of metastable  $\text{Ar}_n^+$  clusters is the loss of the single Ar atoms. The products from this decay channel are observed with a signal-to-noise ratio of 20, which limits the occurrence of unobserved channels, e.g., the loss of Ar dimers, to  $< 5\%$ . Detailed experiments on the decay of metastable  $\text{Ar}_n^+$  clusters<sup>11,55</sup> are also consistent with the loss of single atoms. The excitation energy in these metastable clusters is small compared to the excitation energy of the photoexcited clusters. This suggests that the metastable ionic clusters are more likely to eject neutral clusters than the photoexcited ionic clusters. Since the loss of neutral clusters is not observed from metastable clusters, the decay of the photoexcited clusters via neutral cluster ejection is highly unlikely.

The data in Fig. 7 also provide a basis for obtaining an upper limit to the  $\text{Ar}_k^+ - \text{Ar}$  dissociation energy in the limit of large  $k$ . In the cluster size regime where the average number of neutral atoms lost is both cluster size independent and linearly dependent on the excitation energy, we can safely assume that the dynamics of fragmentation are independent of initial cluster size. Therefore, we can determine an upper bound to the dissociation energy in this regime. The average number of neutral atoms lost reaches an asymptotic value of 21.8 for 1.77 eV (700 nm) excitation and 19.4 for 1.55 eV (820 nm) excitation. The slope of a line connecting these two points is 90 meV per Ar atom lost and predicts that the asymptotic value of the average number of neutral atoms lost for 2.33 eV (532 nm) excitation is approximately 26. The average number of neutral atoms lost following 2.33 eV excitation never exceeds this value, indeed the data appear to be leveling off at this value above  $\text{Ar}_{55}^+$ . An asymptote similar to those seen for the lower energy excitations is not apparent because the largest cluster ion studied in these experiments was  $\text{Ar}_{60}^+$ . We conclude that 90 meV is an upper bound to the  $\text{Ar}_k^+ - \text{Ar}$  dissociation energy.

The upper limit to the  $\text{Ar}_k^+ - \text{Ar}$  dissociation energy obtained above is a convolution of the cluster ion binding energy and the kinetic energy of each departing neutral atom. Experimentally we cannot deconvolute these two components. Engelking<sup>37</sup> has used a statistical (RRK) model to interpret the photofragmentation behavior of  $(\text{CO}_2)_n^+$  clusters<sup>28</sup> (behavior similar to that reported here) and obtains qualitative agreement with the experimental results. Of particular relevance here is the value obtained for the average kinetic energy of each departing molecule in the photofrag-

mentation of  $(\text{CO}_2)_n^+$  clusters, 45 meV. Since the model ignores both the rotation and internal vibrations of the  $\text{CO}_2$  molecules, we can use 45 meV as an estimate for the average kinetic energy of neutral atoms evaporating from the  $\text{Ar}_n^+$  clusters. This places the  $\text{Ar}_k^+ - \text{Ar}$  dissociation energy at approximately 45 meV. The average binding energy of neutral  $\text{Ar}_n$  clusters has been calculated to be approximately 50 meV for  $n > 20$ .<sup>56</sup> Comparison of these two dissociation energies suggests that for cluster ions larger than  $\text{Ar}_{20}^+$ , and perhaps even for smaller cluster ions, the charge does not have a major effect on the  $\text{Ar}_k^+ - \text{Ar}$  dissociation energy and that the forces involved in binding are similar to those in a neutral cluster.

The Engelking model<sup>37</sup> also offers a convincing explanation for the observed width of the ionic photofragment distributions. The model relates the width of the fragment distribution to the ratio of the thermal energy carried off per monomer (at a temperature characteristic of the photoexcited cluster) to the monomer binding energy. Thus the width of the photofragment distribution should increase with increasing excitation energy. This prediction is confirmed by examining the distributions following 2.33 and 1.55 eV excitation (see Fig. 6), where the distribution is approximately 6(5) monomers wide (FWHM) for 2.33(1.55) eV excitation. Comparison of the widths of the ionic photofragment distributions from  $\text{Ar}_n^+$  and  $(\text{CO}_2)_n^+$  at the same excitation energies (2.33 eV) also supports this explanation. The  $(\text{CO}_2)_k^+ - \text{CO}_2$  dissociation energy is approximately 150 meV,<sup>37</sup> three times that of  $\text{Ar}_k^+ - \text{Ar}$ . Assuming equivalent heat capacities for the two systems, the ionic fragment distribution would be expected to be larger from the  $\text{Ar}_n^+$  clusters as is observed [about two monomers wide for  $(\text{CO}_2)_n^+$  vs six for  $\text{Ar}_n^+$ ].

Examination of the abundance anomalies present in the ionic photofragment distributions (e.g.,  $\text{Ar}_{20}^+$  in both Figs. 5 and 6) offers some insight into the abundance anomalies present in the initial mass spectrum (Fig. 2). The utility of such a comparison has been previously demonstrated on  $(\text{CO}_2)_n^-$  clusters.<sup>30</sup> Since the photofragmentation of each initial cluster ion yields only a single photofragment ion, we sum all of the ionic photofragments from *all* of the initial cluster ions to compare with the initial mass spectrum, viz.,

$$I_m = \sum_{j=1}^{60} I_j,$$

where  $I_m$  is the total intensity of the  $\text{Ar}_m^+$  photofragment,  $I_j$  is the intensity of  $\text{Ar}_m^+$  from initial cluster ion  $\text{Ar}_j^+$  and the summation index  $j$  runs over the entire initial cluster ion distribution. A plot of the total photofragment intensity vs cluster size is displayed in Fig. 8. A representation of the initial mass spectrum of Fig. 2 is also shown in Fig. 8. This representation was generated by fitting the envelope of intensities in Fig. 2 to a Gaussian and normalizing it to the total photofragment intensity at  $\text{Ar}_{15}^+$ . The two mass spectra have similar abundance anomalies, as is especially clear for the region near  $\text{Ar}_{20}^+$ .

The similarities in the initial and regenerated mass spectra can be readily understood by examining the formation

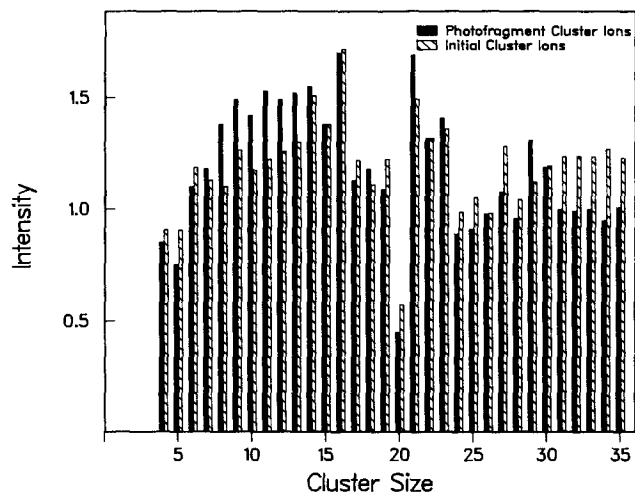


FIG. 8. Summed photofragment mass spectrum and initial cluster ion mass spectrum. See the text for details.

mechanisms for both distributions. As discussed above, the larger cluster ions are formed only when the electron beam intersects the expansion as close to the nozzle orifice as possible. This observation and earlier experiments<sup>40</sup> indicate that the large cluster ions are formed primarily by sequential ion–molecule association reactions while drifting with the free jet expansion. We have also demonstrated that photofragmentation proceeds primarily via single atom evaporation. Since the abundance anomalies generated by both processes are similar, it is virtually certain that they are determined by the energetics of the cluster ions and are not limited by any kinetic processes. If there were a kinetic barrier to the formation of a specific cluster ion, different abundance anomalies would result depending on whether the cluster ion was nucleating or evaporating. This interpretation can also explain the mass spectra observed in the electron impact ionization of neutral  $\text{Ar}_n$  clusters in a collisionless region.<sup>5,6,9,11,42</sup> In these cases ionization causes sufficient fragmentation to yield a distribution of cluster ions determined by the relative stability of the ions: a distribution largely insensitive to the distribution of neutral clusters.

#### IV. CONCLUSION

We have presented an extensive set of measurements on the photophysical properties of the  $\text{Ar}_n^+$  cluster ions. The data were obtained by mass selecting the cluster ion of interest prior to interaction with laser radiation, and mass analyzing and detecting the resulting ionic photofragments. Interpretation of the data yields the following conclusions:

(1) The small  $\text{Ar}_n^+$  ( $n = 4\text{--}15$ ) cluster ions have photophysical properties resembling those of  $\text{Ar}_3^+$ , while the larger  $\text{Ar}_n^+$  ( $n = 20\text{--}40$ ) cluster ions exhibit different photophysical properties, possibly attributable to a central tetramer ion. The transition in the photophysical properties occurs smoothly over a relatively narrow cluster size range ( $n = 15\text{--}20$ ). In particular, none of the cluster ions studied have photophysical properties which resemble those of  $\text{Ar}_2^+$ .

(2) Photofragmentation proceeds via the photodisso-

ciation of the central ion within the cluster, followed by the capture of the nascent fragments to effect energy redistribution. At least for the large cluster ions, energy redistribution leads primarily to the sequential loss of Ar atoms via an evaporative mechanism. From this model we determine that the  $\text{Ar}_k^+ \text{--Ar}$  dissociation energy is  $\leq 90$  meV. An estimate of the kinetic energy of the ejected atoms yields a value of approximately 45 meV for the dissociation energy. This value is comparable to calculated values for the *neutral*  $\text{Ar}_k \text{--Ar}$  dissociation energy. It therefore seems likely that atoms on the surface of large ( $n \geq 20$ ) ionic clusters do not interact strongly with the central ionic core.

(3) Examination of the ionic photofragment distributions shows that the abundance anomalies in the initial mass spectrum are determined by the energetics of the cluster ions. The photoabsorption cross section measurements also exhibit “anomalous” behavior near  $\text{Ar}_{20}^+$  (the most obvious abundance anomaly), indicative of the intimate connection between the changes in electronic structure and in bond strength as a function of cluster size.

Finally, we emphasize that the large change in photoabsorption cross section occurs over a relatively narrow range of cluster size. We have observed similarly abrupt changes in photofragmentation behavior vs cluster size in the photofragmentation of  $(\text{CO}_2)_n^-$  and  $\text{Br}_2^-(\text{CO}_2)_n$  clusters.<sup>30,38</sup> These results demonstrate the importance of measurements on mass selected clusters, since such abrupt transitions, which are clearly important to an understanding of the transition from gas phase to condensed phase behavior, would most likely be heavily smoothed by experiments employing limited mass selectivity.

#### ACKNOWLEDGMENTS

This research was supported by NSF Grant Nos. CHE83-16628 and PHY86-04504. We are pleased to acknowledge very useful and stimulating discussions with P. C. Engelking.

<sup>1</sup>M. R. Hoare and P. Pal, *Adv. Phys.* **20**, 161 (1971); M. R. Hoare, *Adv. Chem. Phys.* **40**, 49 (1979).

<sup>2</sup>J. C. Phillips, *Chem. Rev.* **86**, 619 (1986), and references therein.

<sup>3</sup>T. D. Mark and A. W. Castleman, Jr., *Adv. At. Mol. Phys.* **20**, 65 (1985); in *Gaseous Ion Chemistry and Mass Spectrometry*, edited by J. H. Futrell (Wiley, New York, 1986), p. 259, and references therein.

<sup>4</sup>U. Buck and H. Meyer, *Phys. Rev. Lett.* **52**, 109 (1984); *Ber. Bunsenges. Phys. Chem.* **88**, 254 (1984); *J. Chem. Phys.* **84**, 4854 (1986).

<sup>5</sup>D. R. Worsnop, S. J. Buelow, and D. R. Hershbach, *J. Phys. Chem.* **88**, 4506 (1984).

<sup>6</sup>H. P. Birkhofer, H. Haberland, M. Winterer, and D. R. Worsnop, *Ber. Bunsenges. Phys. Chem.* **88**, 207 (1984).

<sup>7</sup>D. Kreisler, O. Echt, M. Knapp, and E. Recknagel, *Phys. Rev. A* **33**, 768 (1986).

<sup>8</sup>L. Friedman and R. J. Beuhler, *J. Chem. Phys.* **78**, 4669 (1983).

<sup>9</sup>A. J. Stace and C. Moore, *Chem. Phys. Lett.* **96**, 80 (1983); A. J. Stace, *ibid.* **113**, 355 (1985).

<sup>10</sup>I. A. Harris, R. S. Kidwell, and J. A. Northby, *Phys. Rev. Lett.* **53**, 2390 (1984).

<sup>11</sup>T. D. Mark, P. Scheier, K. Leiter, W. Ritter, K. Stephan, and A. Stamatovic, *Int. J. Mass Spectrom. Ion. Proc.* **74**, 281 (1986).

<sup>12</sup>O. Echt, M. C. Cook, and A. W. Castleman, *Chem. Phys. Lett.* **135**, 229 (1987).

<sup>13</sup>J. M. Soler, J. J. Sáenz, N. Garcia, and O. Echt, *Chem. Phys. Lett.* **109**, 71 (1984); J. J. Sáenz and N. Garcia, *ibid.* **114**, 15 (1985); J. J. Sáenz, J. M.

- Soler, and N. Garcia, *Surf. Sci.* **156**, 121 (1985).
- <sup>14</sup>E. E. Polymeropoulos and J. Brickmann, *Surf. Sci.* **156**, 563 (1985); E. E. Polymeropoulos, S. Löffler, and J. Brickmann, *Z. Naturforsch. Teil A* **40**, 516 (1985).
- <sup>15</sup>H. Haberland, *Surf. Sci.* **156**, 305 (1985).
- <sup>16</sup>J. Hesslich and P. J. Kuntz, *Z. Phys. D* **2**, 251 (1986).
- <sup>17</sup>L. Jansen and R. Block, in *PDMS and Clusters, Proceedings of the First International Workshop on the Physics of Small Systems*, edited by E. R. Hilf, F. Kammer, and K. Wien (Springer, Berlin, 1987), p. 151.
- <sup>18</sup>H.-U. Böhmer and S. Peyerimhoff, *Z. Phys. D* **8**, 91 (1988).
- <sup>19</sup>P. J. Kuntz and J. Valldorf, *Z. Phys. D* **8**, 195 (1988).
- <sup>20</sup>M. Amarouche, G. Durand, and J. P. Malrieu, *J. Chem. Phys.* **88**, 1010 (1988).
- <sup>21</sup>C. E. Moore, *Atomic Energy Levels*, Nat. Stand. Ref. Data Ser. Circ. No. 467 (U. S. GPO, Washington, D. C., 1948).
- <sup>22</sup>L. C. Lee, G. P. Smith, T. M. Miller, and P. C. Cosby, *Phys. Rev. A* **17**, 2005 (1978).
- <sup>23</sup>J. A. Vanderhoff, *J. Chem. Phys.* **68**, 3311 (1978); L. C. Lee and G. P. Smith, *Phys. Rev. A* **19**, 2329 (1979).
- <sup>24</sup>W. J. Stevens, M. Gardner, A. Karo, and P. Julienne, *J. Chem. Phys.* **67**, 2860 (1977).
- <sup>25</sup>W. R. Wadt, *J. Chem. Phys.* **73**, 3915 (1980).
- <sup>26</sup>N. E. Levinger, D. Ray, K. K. Murray, A. S. Mullin, C. P. Schulz, and W. C. Lineberger, *J. Chem. Phys.* **89**, 71 (1988).
- <sup>27</sup>H. Helm and R. Möller, *Rev. Sci. Instrum.* **54**, 837 (1983).
- <sup>28</sup>M. L. Alexander, M. A. Johnson, and W. C. Lineberger, *J. Chem. Phys.* **82**, 5288 (1985).
- <sup>29</sup>L. A. Bloomfield, R. R. Freeman, and W. L. Brown, *Phys. Rev. Lett.* **54**, 2246 (1985).
- <sup>30</sup>M. L. Alexander, M. A. Johnson, N. E. Levinger, and W. C. Lineberger, *Phys. Rev. Lett.* **57**, 976 (1986).
- <sup>31</sup>P. J. Brucat, L.-S. Zheng, C. L. Pettiette, S. Yang, and R. E. Smalley, *J. Chem. Phys.* **84**, 3078 (1986).
- <sup>32</sup>Y. Liu, Q.-L. Zhang, F. K. Tittel, R. F. Curl, and R. E. Smalley, *J. Chem. Phys.* **85**, 7434 (1986).
- <sup>33</sup>W. L. Brown, R. R. Freeman, K. Raghavachari, and M. Schlüter, *Science* **235**, 860 (1987).
- <sup>34</sup>M. E. Geusic, M. F. Jarrold, T. J. McIlrath, R. R. Freeman, and W. L. Brown, *J. Chem. Phys.* **86**, 3862 (1987).
- <sup>35</sup>S. C. O'Brien, J. R. Heath, R. F. Curl, and R. E. Smalley, *J. Chem. Phys.* **88**, 220 (1988).
- <sup>36</sup>C. Bréchnignac, P. Cahuzac, and J.-P. Roux, *J. Chem. Phys.* **88**, 3022 (1988).
- <sup>37</sup>P. C. Engelking, *J. Chem. Phys.* **85**, 3103 (1986).
- <sup>38</sup>M. L. Alexander, N. E. Levinger, M. A. Johnson, D. Ray, and W. C. Lineberger, *J. Chem. Phys.* **88**, 6200 (1988).
- <sup>39</sup>M. L. Alexander, Ph.D. thesis, University of Colorado, 1987.
- <sup>40</sup>M. A. Johnson, M. L. Alexander, and W. C. Lineberger, *Chem. Phys. Lett.* **112**, 285 (1984).
- <sup>41</sup>B. A. Mamyrin, V. I. Karataev, D. V. Shmikk, and V. A. Zagulin, *Sov. Phys. JETP* **37**, 45 (1973).
- <sup>42</sup>A. Ding and J. Hesslich, *Chem. Phys. Lett.* **94**, 54 (1983).
- <sup>43</sup>W. R. Wadt, *Appl. Phys. Lett.* **38**, 1030 (1981).
- <sup>44</sup>P. G. LeComber, R. J. Loveland, and W. E. Spear, *Phys. Rev. B* **11**, 3124 (1975).
- <sup>45</sup>S. D. Druger and R. S. Knox, *J. Chem. Phys.* **50**, 3143 (1969).
- <sup>46</sup>K. S. Song, *Can. J. Phys.* **49**, 26 (1971).
- <sup>47</sup>W. E. Spear and P. G. LeComber, in *Rare Gas Solids*, edited by M. L. Klein and J. A. Venables (Academic, New York, 1977), Vol. 2, p. 1119.
- <sup>48</sup>M. Umehara, *Phys. Rev. B* **33**, 4237, 4245 (1986).
- <sup>49</sup>See AIP document no. PAPS JCPA-89-5654-3 for 3 pages of photofragmentation product distributions presented in Fig. 6 (and the data at 1.77 eV). Order by PAPS number and journal reference from American Institute of Physics, Physics Auxiliary Publication Service, 335 East 45th Street, New York, NY 10017. The price is \$1.50 for each microfiche (98 pages) or \$5.00 for photocopies of up to 30 pages, and \$0.15 for each additional page over 30 pages. Airmail additional. Make checks payable to the American Institute of Physics.
- <sup>50</sup>C. E. Klots, *Z. Phys. D* **5**, 83 (1987).
- <sup>51</sup>F. G. Amar and B. J. Berne, *J. Phys. Chem.* **88**, 6720 (1984).
- <sup>52</sup>F. G. Amar, in *The Chemistry and Physics of Small Clusters*, edited by P. Jena, S. Khanna, and B. Rao, NATO ASI Series (Plenum, New York, 1987), p. 207.
- <sup>53</sup>D. L. Turner and D. C. Conway, *J. Chem. Phys.* **71**, 1899 (1979).
- <sup>54</sup>R. G. Keesee and A. W. Castleman, Jr., *J. Phys. Chem. Ref. Data* **15**, 1011 (1986).
- <sup>55</sup>A. J. Stace, *J. Chem. Phys.* **85**, 5774 (1986); (submitted).
- <sup>56</sup>M. R. Hoare and P. Pal, *Adv. Phys.* **24**, 645 (1975).